# Reliability of a MEMS Torsional Ratcheting Actuator

Danelle M. Tanner, Jeremy A. Walraven, Stephen M. Barnes[⊕], Norman F. Smith, Fernando Bitsie, Scot E. Swanson

Sandia National Laboratories, P.O. Box 5800, MS 1081, Albuquerque, NM 87185-1081
http://www.mems.sandia.gov     email: tannerdm@sandia.gov
[⊕]MEMX, Inc., 5600 Wyoming Blvd. NE, Suite 20, Albuquerque, NM 87109

## ABSTRACT

A new surface-micromachined actuator, the Torsional Ratcheting Actuator (TRA) has been characterized and stress tested for reliability. The most prominent failure mechanism when running at high speeds (ratcheting frequencies of 333, 1000, or 3000 Hz) is wear on rubbing surfaces leading to adhesion between the ring gear and the alignment guide. We have also observed failure when running at low speeds (5 Hz) due to misalignment of the ring gear preventing the ratchet pawl from engaging.

A wear model was developed which closely predicts the normal force promoting the wear and is in agreement with supporting calculations.

We observed multiple ratcheting in the TRA during calibration and solved the equations of motion to confirm that it was due to the moment of inertia of the large ring gear. Damping was shown to have an effect also.

## INTRODUCTION

An element of the success of MicroElectroMechanical Systems (MEMS) as they reach commercialization depends on reliability studies and predictive modeling. The TRA [1] was developed at Sandia National Laboratories as a low-voltage alternative to the microengine; both are used to drive many different types of devices from gear trains to pop-up mirrors [2]. The TRA can be operated with less complex drive signals (square wave, sine wave, sawtooth) than the microengine, which requires model-based drive signals [3]. The TRA has minimal rubbing surfaces and will not trap wear debris as the microengine did in the hub and pin joint area [4]. The design of the TRA maximizes comb finger density leading to increased output power density. The TRA has a smaller footprint than the microengine, taking up about 1/6 the area. As was demonstrated earlier, wear of rubbing surfaces was the significant failure mechanism in microengines [5] and is a concern here. We normally count number of gear rotations in our experiments, but because the TRA gear (radius of 400 μm) is ten times larger than the microengine gear (radius of 40 μm), total linear displacement should be the value for comparison between the two.

The overall purpose of these experiments was to determine the failure modes and mechanisms of the TRA and attempt to describe the mechanisms through a model. An understanding of the failures should lead to a better design. A secondary objective was to compare the results to the microengine to determine if the TRA is a viable alternative.

## EXPERIMENTAL APPROACH

### Sample Preparation

Surface micromachined MEMS are mechanical structures fabricated from deposited thin films. The structures are encased in sacrificial layers (typically $SiO_2$) until ready for use. The oxide film is etched away using hydrofluoric acid (HF) to yield a "released" sample. There are several strong adhesive forces that act on the structures during the drying stage of the release [6]. These include the dominant capillary forces, electrostatic forces, and van der Waals forces [7]. Coupling agent coatings such as alkysilanes have been used to increase the hydrophobicity of the polysilicon surface, thus eliminating capillary forces [8, 9]. Application of a coupling agent requires preparation of the polysilicon surface by an oxidation step ($H_2O_2$), resulting in an oxide layer a few nanometers thick. The samples in this experiment were coated with such an alkysilane coupling agent.

### TRA Operation

The TRA uses rotational comb drives for electrostatic operation, which is similar to previous gyro designs [10, 11]. A large circular frame ties the movable banks of combs together. A SEM image of the fabricated device is shown in Figure 1. Four cantilever beams
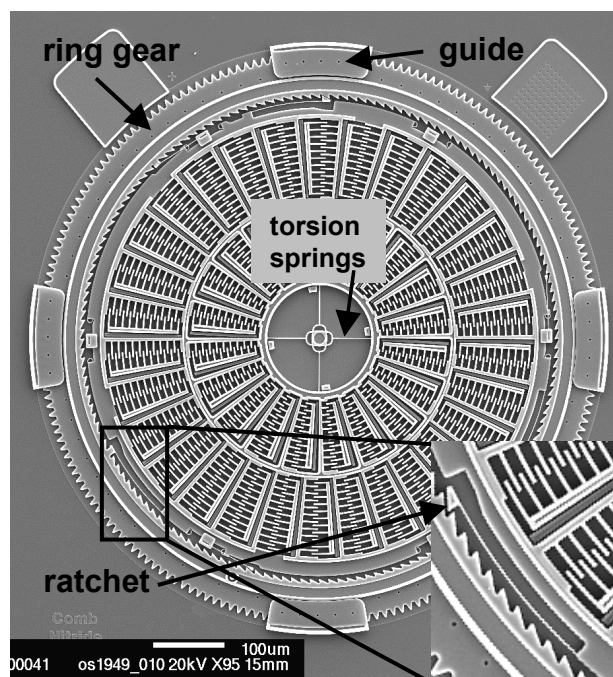


**Figure 1**. This SEM image of the fabricated torsional ratcheting actuator shows the ratchet and ring mechanisms. The inset shows an enlarged view of the ratchet.

support this frame in its center and act as the frame's spring return. These four beams are stiff to any lateral motion of the frame but compliant to rotation. There are three ratchet pawls and three anti-reverse pawls (see Figure 2) located symmetrically around the ring gear. Four guides are used to maintain alignment of the ring gear, constraining motion along the x, y, and z planes.

For operation, a periodic voltage is applied between the stationary and moving combs. As the voltage increases, the torsion frame rotates counter-clockwise about its springs in response to the electrostatic attraction. As the frame begins to rotate, the ratchet pawls engage the ring gear and cause it to rotate also. As the gear is rotating, the anti-reverse pawls are forced out of their engagement with the ratchet teeth. Once the ring gear has moved sufficiently, the anti-reverse pawls engage the next tooth. When the voltage is removed, the central torsion springs force the frame to return to its rest position. As the frame is returning, the ratchet pawls attempt to drag the ring gear in the reverse direction via friction of the ratchet pawls with the ring gear. Because the anti-reverse mechanisms have engaged, the ratchet pawls are forced to skip over the tooth and finally engage the next tooth. At this point, the frame has returned to its initial position, and the cycle can be repeated. TRA operation requires 160 voltage pulses to make a complete rotation of the gear, assuming one click of the gear per drive signal pulse.

The TRA design is very robust and proper functioning can be achieved with many different types of voltage pulses. The TRAs were driven with three basic voltage signals: 1) an offset sine wave, 2) a sawtooth pulse, and 3) a sine wave (Figure 3). The offset sine wave was shifted in phase by 270 degrees and had a DC offset of 16.5 V, which matched its amplitude.

*TRA Calibration*

We have observed multiple stepping of the ratchet pawl at most frequencies. Multiple stepping occurs when the ratchet pawl engages more than one tooth per drive signal pulse. The multiple stepping changes the typical calibration of one rotation per 160 pulses.
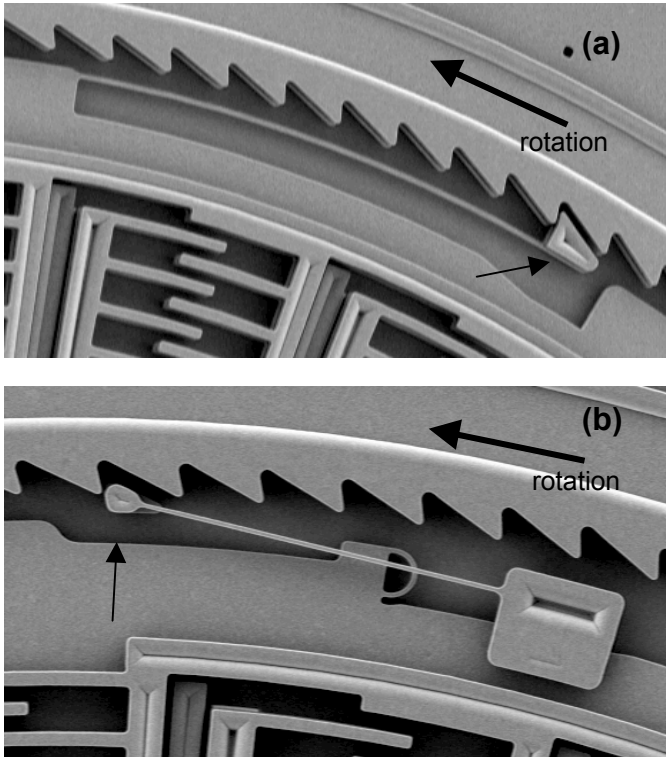
In order to understand this effect, we tested the reaction of five separate TRAs to a set number of input pulses while the frequency was varied. Offset sine-wave drive signals with peak amplitude of 33 V at frequencies of 50, 100, 333, 1000, and 3000 Hz activated the comb frame. We used 10, 20, or 30 input pulses and observed the number of clicks the gear rotated (160 clicks is a full rotation). The data are shown in Figure 4. There is a general trend in the data (neglecting 1000 Hz) that as the frequency increases, the multiple ratcheting decreases. This may be due in part to the fact that the ring gear has no load and therefore has little to slow it down. The ring gear eventually stops due to friction against the alignment guides, ratchet pawls, and the dimples on the bottom surface. The 1000 Hz signal does not follow the trend, but we will address that problem in the
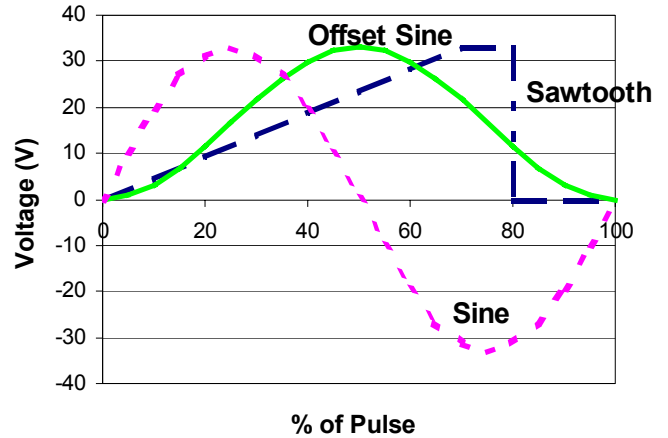


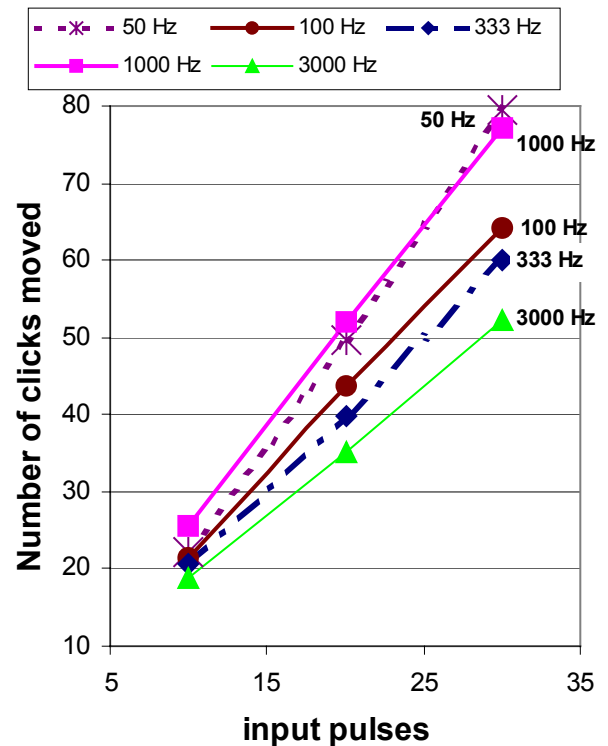**Figure 3.** The three types of drive signals used in the experiments



**Figure 4.** This calibration data demonstrates the multiple stepping problem of the TRA running without a load. The amplitude of the offset sine-wave drive signal was 33 V.



**Figure 2**. SEM images of the (a) ratchet pawl, and (b) anti-reverse pawl. The rotation direction of the ring gear is shown by the arrow.

next section where we model the motion.

We used these calibration curves to calculate the gear-rotation factors. The factors were 1.97, 2.58, and 1.66 gear rotations per 160 pulses for the frequencies of 333, 1000, 3000 Hz, respectively. Calibration was also run using the sawtooth and pure sine wave drive signals. Both resulted in similar gear rotation factors of 2, 2.4, and 1.2 per 160 pulses for the frequencies of 333, 1000, 3000 Hz, respectively.

Testing of a TRA with a load gear (at a higher amplitude of 50 V) showed that an increase in frequency lead to an increase in the multiple ratcheting as seen in Figure 5. The trend is the opposite of that observed without a gear implying that the overall moment of inertia has a large effect on the motion. We observed one-to-one ratcheting for all frequencies between 1 Hz and 50 Hz. The slightly higher frequencies of 100 and 200 Hz produced two-to-one ratcheting. The 333 Hz and 1000 Hz drive signals produce higher multiples of ratcheting than the 33 V pulse shown in Figure 4 because of the higher force imparted to the ring gear. Unfortunately, we were unable to test at 3000 Hz due to the possibility of double counting gear rotations.
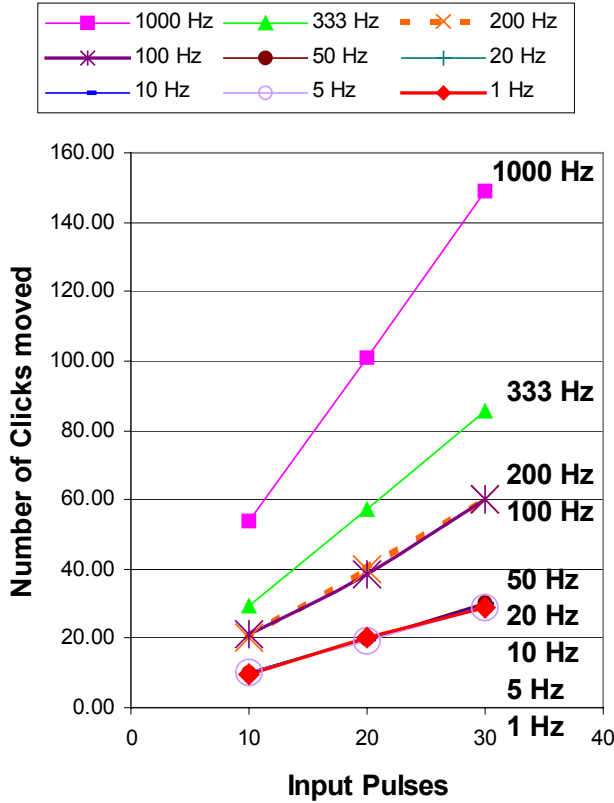


**Figure 5.** This data was taken from a TRA with a load gear attached. The amplitude of the offset sine-wave drive signal was 50 V.

*TRA Model*

We have modeled the actuator section of the TRA and shown that it has a resonance of 5 kHz in previous work [1]. In this section, we determine the effect of the ring gear on the functionality of the TRA. To better understand the TRA's ratcheting behavior, we attempted to describe the ring gear's dynamic behavior with its equations of motion. The equation of motion included: a) the angular acceleration of the ring gear, b) the loss mechanisms of viscous damping and friction forces, and c) an electrostatic torque input due to the TRA comb fingers. The damping constant, $c_d$, represents the damping of the air surrounding the TRA. The friction force due to the dimple-gear interaction was represented by simple sliding and was described for mathematical purposes as $T_f = \mu F(V(t))\sin\theta$. The friction coefficient, $\mu = 0.3$, was used and the $\sin\theta$ yields the force component normal to the surface. Friction forces arise from a number of possible areas: the guide-dimple/ring-gear interaction, the dimple/ground-plane interaction, the TRA ratchet-gear interaction, and the anti-reverse pawl-gear interaction. The equation of motion is given as

$$I\ddot{\theta} + c_d\dot{\theta} = T(t) = T(F(V(t))) - T_f = (1 - \mu\sin\theta)r \cdot F(V(t)) \quad (1)$$

The equation of motion was solved using 'Solution by Variation of Parameters' along with the initial condition of no angular displacement and no angular velocity. The solution expression was a function of voltage amplitude, frequency, mass moment of inertia, damping, friction, and pulse shape. This solution ignores the friction between the gear dimples and the ground plane. The solution is composed of both homogenous and complementary parts as in the following,

$$\theta(t) = [u_1(t)\cdot\theta_1(t) + u_2(t)\cdot\theta_2(t)]_C + [c_1\theta_1(t) + c_2\theta_2(t)]_H \quad (2)$$

where $\theta_1(t) = 1$ and $\theta_2(t) = e^{-\frac{c_d}{I}t}$.

Applying the initial conditions of $\theta(t=0) = 0$ and $\dot{\theta}(t=0) = 0$, the total solution is rewritten as

$$\theta(t) = [u_1(t) - u_1(t=0)]\cdot\theta_1(t) + [u_2(t) - u_2(t=0)]\cdot\theta_2(t), \quad (3)$$

where, $u_1 = -\int \frac{\theta_2}{|W|}T(t)dt$, $u_2 = +\int \frac{\theta_1}{|W|}T(t)dt$, and the Wronskian, $|W|$, is $|W| = -\frac{c_d}{I}\cdot e^{-\frac{c_d}{I}t}$.

The overall torque expression taken from the equation of motion is given as

$$T(t) = r\frac{1}{2}V^2\frac{dC}{d\theta} = (1 - \mu\sin\theta)r\frac{N\varepsilon_0 V^2}{4I}\cdot(3 - 4\cos\omega t + \cos 2\omega t) \quad (4)$$

where $C$ is capacitance between comb fingers. For convenience the expression was rewritten as

$$T(t) = \beta(3 - 4\cos\omega t + \cos 2\omega t), \quad (5)$$

where $\beta = (1 - \mu\sin\theta)r\frac{N\varepsilon_0 V^2}{4I}$. The variables are: $r$, radius, $N$, number of electrostatic comb fingers, $\varepsilon_0$, permitivity constant, $V$, voltage, and $I$, mass moment of inertia of the ring gear. Substituting the torque expression, $T(t)$, into $u_1$ and $u_2$ and evaluating the integral at the given bounds yields,

$$u_1 = -\int_{t=0}^{t=t}\frac{\theta_2}{|W|}T(t)dt = u_1(t) - u_1(t=0) = g_1(t) \quad (6)$$

and $u_2 = \int_{t=0}^{t=t}\frac{\theta_1}{|W|}T(t)dt = u_2(t) - u_2(t=0) = g_2(t).$ \quad (7)

We obtain the following for the given solution bounds,

$$g_1(t) = \frac{\beta}{\frac{c_d}{I}}\left(3t - \frac{4}{\omega}\sin\omega t + \frac{1}{2\omega}\sin 2\omega t\right), \quad (8)$$

and $g_2(t) = g_{21}(t) + g_{22}(t) + g_{23}(t),$ \quad (9)

where

$$g_{21}(t) = \frac{-1}{\frac{c_d}{I}}\left(\frac{3\beta}{\frac{c_d}{I}}\left(e^{\frac{c_d}{I}t} - 1\right)\right), \tag{10}$$

and

$$g_{22}(t) = \frac{1}{\frac{c_d}{I}}\left(\frac{4\beta}{\left(\frac{c_d}{I}\right)^2 + \omega^2}\left\{e^{\frac{c_d}{I}t}\left(\frac{c_d}{I}\cos\omega t + \omega\sin\omega t\right) - \frac{c_d}{I}\right\}\right), \tag{11}$$

and

$$g_{23}(t) = \frac{-1}{\frac{c_d}{I}}\left(\frac{\beta}{\left(\frac{c_d}{I}\right)^2 + 4\omega^2}\left\{e^{\frac{c_d}{I}t}\left(\frac{c_d}{I}\cos 2\omega t + \omega\sin 2\omega t\right) - \frac{c_d}{I}\right\}\right). \tag{12}$$

The general solution can be nicely written in the following form as

$$\theta(t) = g_1(t) \cdot \theta_1(t) + g_2(t) \cdot \theta_2(t). \tag{13}$$

The general solution as a function of frequency was plotted against the TRA experimental data. The offset sine wave drive signal was used for this calculation. The solution was fit by varying the damping constant, $c_d$, for each frequency of 333Hz, 1000Hz, and 3000Hz. The damping coefficients used were $60\times10^{-12}$, $15.5\times10^{-12}$, and $7.5\times10^{-12}$ kg·m²/s for each frequency respectively. The mass moment of inertia of the ring gear was given as $I = 3\times10^{-15} kg \cdot m^2$. Using these values the solution compared to experimental data was plotted in Figure 6. In the 1000 Hz and 3000 Hz cases, the comparisons were close, the slopes varied a little and it was noticed during the fit that the slopes were generally dependent on the damping value. Changing any parameter that changed the torque amplitude could easily offset the fit. The mass moment of
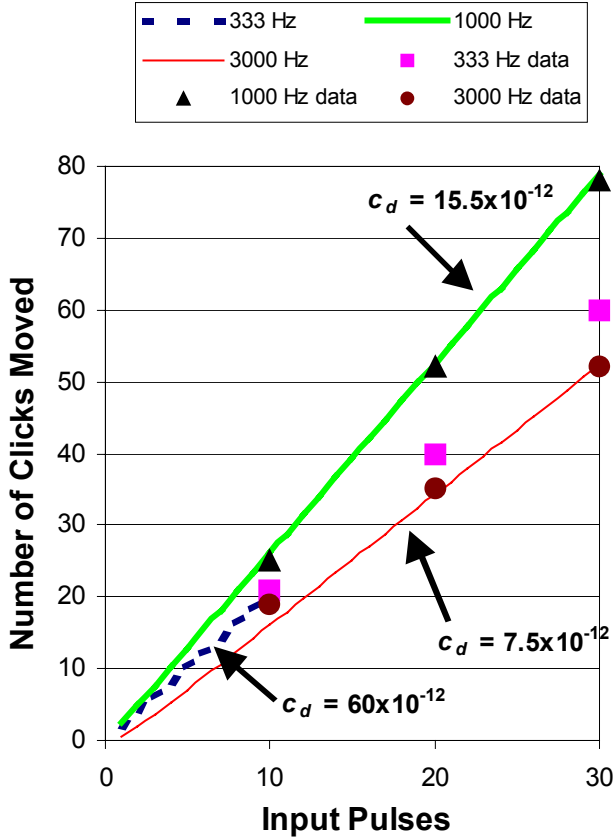


**Figure 6**. Solutions to the equations of motion at these three frequencies show that the moment of inertia and damping are the source of multiple ratcheting. The units for $c_d$ are kg·m²/s.

inertia, $I$, is a measure of how much energy was in the system before the loss mechanisms stopped the system from moving. In the 333 Hz case, the slope and amplitude of the comparisons were valid for only eleven pulses. For higher values of input pulses, the model fails to produce output. This failure at 333 Hz may be due to the lower frequency operation coupled with our simplification of the electrostatic forces. The lower frequency yields a small $I\ddot{\theta}$ term in the equations of motion allowing the stopping forces to have a larger effect. Additionally, a nonlinear term in the electrostatic force equation was neglected in the calculations.

*Reliability Tests*

The TRA used in this experiment was the best-functioning design of many on a test die. The dice were packaged with taped glass covers to prevent particle contamination during handling. The packages were then stored in a dry nitrogen environment prior to testing. The covers were removed during the test to expose the microengines to the local environment. The Sandia High Volume Measurement of Micromachine Reliability (SHiMMeR) [12] tester was used to provide electrical signals to large numbers of packaged microengines and to optically inspect them for functionality.

A controlled humidity environment was achieved by bubbling laboratory compressed air through a large bottle of deionized water. The humid air that exited the bottle was then piped into the environmental chamber surrounding the packaged parts. A humidity sensor located inside the chamber controlled the airflow to maintain humidity levels to within ±1 % RH at 25°C. A General Eastern humidity monitor (Model HYGRO M4) using chilled mirror technology measured the dew point. We performed lifetime tests at the controlled value of 35% RH at an average ambient temperature of 23.6°C.

We performed two types of reliability tests; one in which we looked at frequency dependence and one to investigate wear. In all of the tests, the TRAs were stressed until failure. The devices were exercised at stress speed and then slowed to 5 Hz to inspect for functionality. For the first test, a failure was defined as the inability of the large ring gear to make a complete revolution at the 5 Hz inspection speed. During the inspection interval, we noted any changes or degradation in the motion of the gear. If the TRA passed, the duration of the next stress period was doubled. In the wear test, we were looking for failures due to adhesion from the wear process, so we changed the failure definition to no movement in the ring gear at the inspection speed or high speed.

*Frequency Test:* We wanted to avoid stressing near the resonant frequency of 5000 Hz, so we initially chose 3000 Hz, which was safely under it. The other frequencies were simply a factor of 3 smaller. Thus, we chose frequencies of 333 Hz, 1000 Hz, and 3000 Hz and stressed 14, 10, and 15 TRAs, respectively. The sawtooth pulse shape drive signal with amplitude of 33V was used. The amplitude of 33 V was selected because it is roughly 20% higher than the minimum operating voltage measured from a sample of TRAs.

*Wear test:* We released and coated TRAs from a different wafer from the same lot as the initial test. We stressed 19 devices at 333 Hz, driving them with the offset sine wave to study the effects of wear.

## RESULTS AND DISCUSSION

*Frequency Test*

The frequency experiments were designed to determine failure modes with a new design. As mentioned earlier, the failure defini-

tion for these experiments was no ring gear motion at the inspection speed of 5 Hz. Typically, we observed center actuator motion and slight back and forth motion of the ring gear for these inspection-speed failures. Results are shown in Figure 7 with lognormal fits to the unimodal and bimodal distributions. Table 1 lists the median number of gear rotations to failure, $t_{50}$, and the slope parameter, $\sigma$. Both lower and upper median values are included for the bimodal distributions.

**Table 1**. Median number of gear rotations to failure.

| Test | Lower | | Upper | |
|---|---|---|---|---|
| | $t_{50}$ | $\sigma$ | $t_{50}$ | $\sigma$ |
| 333 Hz | $3.0 \times 10^4$ | .24 | $7.0 \times 10^5$ | .15 |
| 1000 Hz | $1.3 \times 10^3$ | 1.0 | $1.8 \times 10^5$ | .3 |
| 3000 Hz | $1.1 \times 10^6$ | 2.1 | | |

The bimodal distribution of the 333 Hz experiment indicated a shift in the population at 42% failed. The 1000 Hz distribution appears to have two failure modes due to the large change in the slope parameter. Both bimodal distributions are characteristic of two different failure modes. The lower distributions failed by a misalignment in the ring that caused the non-engagement of the ratchet while operating at the 5 Hz inspection speed. The upper distributions were failures due to wear and adhesion of the ring gear. We fit the 3000 Hz data with a unimodal fit, which yields the largest value of median pulses to failure, but it has an alarmingly high slope parameter. This experiment was stopped with only 45% failed because none of the parts still on test were functioning at high speed, effectively removing the stress. They all functioned at the inspection speed of 5 Hz. This failure at high speed was different from the other two frequencies. It may be explained in light of recent data [13] that found a resonance near 3000 Hz. Operating at resonance will amplify the displacements, which may have lead to the high-speed failures.

The failures described at low frequency produce a "wiggling" behavior, where the comb drive actuates, but the ring gear does not complete a revolution. Preliminary investigations did not reveal the presence of broken elements, foreign material, debris, or contamination, obstructing the motion of the electrostatic actuator.

In failures such as these, the ratchet pawls have been observed sticking to the ring gear (via friction) moving the gear slightly forward and backward. The presence of the anti-reverse pawls prevents the ring gear from moving back a complete "click". However, the
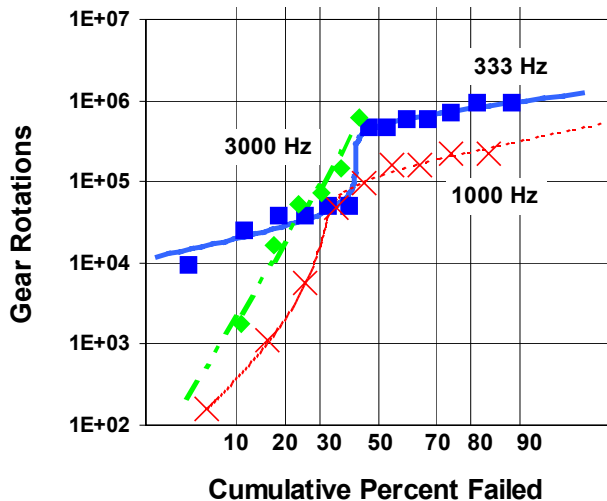
anti-reverse pawls do not prevent the ring gear from moving backwards a fraction of a "click," or a distance less than 5 μm. Misalignment of the ring gear may also prevent the ratchet pawls from engaging the TRA, and occasionally the ratchet pawl may engage the ring gear causing the ring gear to move several clicks prior to wiggling again. Misalignment of the ring gear itself may prevent one of the three ratchet pawls from engaging.

Closer examination of a "wiggling" TRA revealed a ratchet pawl not in contact with the ring gear, leaving only two ratcheting pawls and three anti-reverse pawls in contact with the ring gear. Such displacement of the ring gear may not allow the two contacting ratchet pawls to engage. The friction between the ratchet pawls, anti-reverse pawls, and the ring gear may induce motion of the ring gear in a wiggling fashion. Figure 8, a and b, show misalignment of
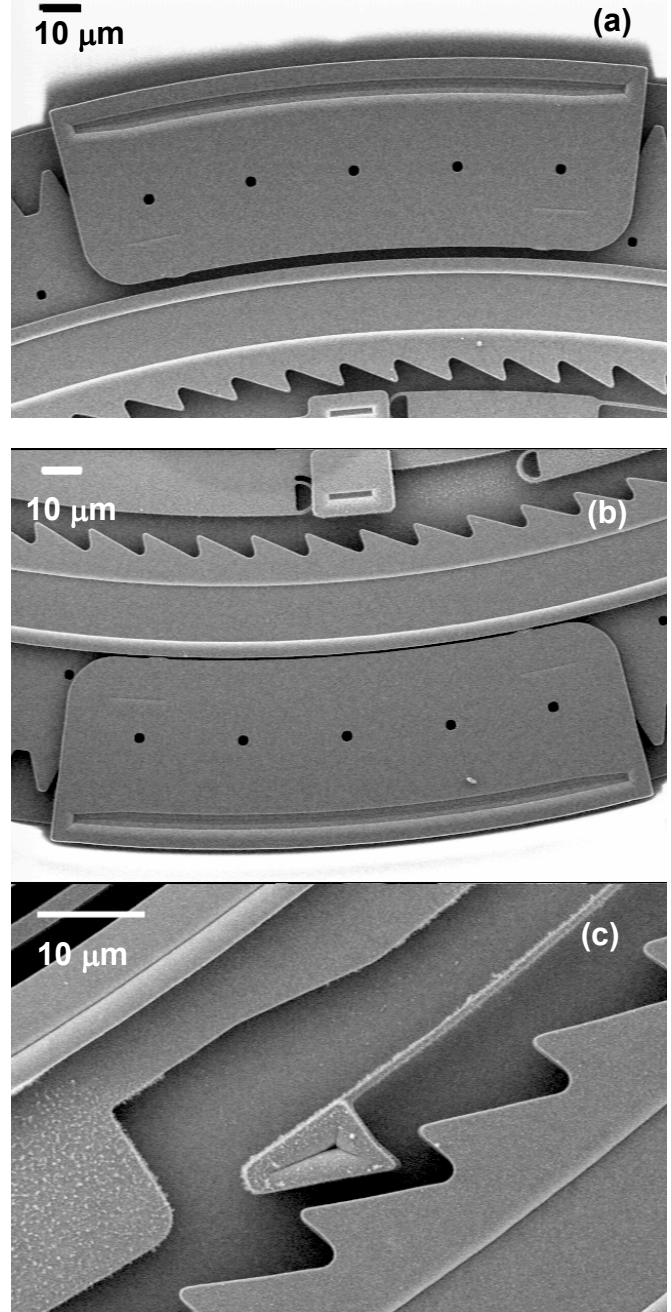






**Figure 8**. SEM images illustrating gear misalignment along the (a) top guide, large gap, (b) bottom guide revealing contact between the guide and ring gear, and (c) gap between a ratchet pawl and ring gear.



**Figure 7**. The frequency data for TRAs operated with the sawtooth drive signal is shown with bimodal fits.

the ring gear with the guide. In this example, all 3 of the ratchet pawls were not engaging the next tooth. When the ring gear is misaligned, the ratchets have to extend further than intended to engage the ring gear. Overall, the friction between the ratchet pawls and the ring gear can cause the gear to wiggle during operation of the electrostatic actuator.

A major area of concern with the frequency data is the fact that failures at the inspection speed of 5 Hz typically ran at the stress speed. This was completely opposite to our experience with microengines that typically fail at high speed before they fail at the inspection speed. Because the devices were not removed from the stressing apparatus, they continued to run at high speed accumulating more cycles after being diagnosed as failing at the inspection speed. It is entirely possible that the TRAs we examined had run close to the maximum number of cycles for the entire test. That number would be $10^5$ gear rotations for the 333 Hz test, $10^6$ gear rotations for the 1000 Hz test and $9.6 \times 10^5$ gear rotations for the 3000 Hz test.

Failure analysis from a TRA that failed at $9.5 \times 10^5$ gear rotations (running at 1000 Hz) indicated that the ring gear is in close contact to guide dimples as seen in Figure 9. These dimples are used to maintain alignment of the ring gear. There should be 0.5-micron clearance. We performed a cross section of the dimple-ring contact area using a Focused Ion Beam (FIB) and the result is shown in Figure 10. In the circled region the two-polysilicon surfaces have adhered. We also performed a cross section of the lower guide dimple and saw no adhesion.

Analysis of a TRA stressed at 3000 Hz reveals adhesion of the ring gear to the alignment guide dimples. Another FIB cut performed along the contact region revealed adhesion between the ring gear and the alignment guide dimple. This ratchet had $6.2 \times 10^5$ gear rotations accumulated before failure. The failure mechanism for this sample is consistent with the failure mechanism observed in the previous TRA (1000 Hz).

Failure analysis of four failed TRAs at 333 Hz revealed adhesion of the ring gear to the constraining dimples similar to Figure 10. This adhesion was observed independent of the number of apparent rotations accumulated by the TRA (Figure 7). Because the parts continued to be stressed to roughly $10^5$ rotations after they were labeled failed and before they were subjected to failure analysis, they eventually failed due to wear and adhesion (the same as failures described in the next section).

Throughout the frequency experiments we observed TRAs that ran at high speed but did not ratchet at low speed. All of the drive
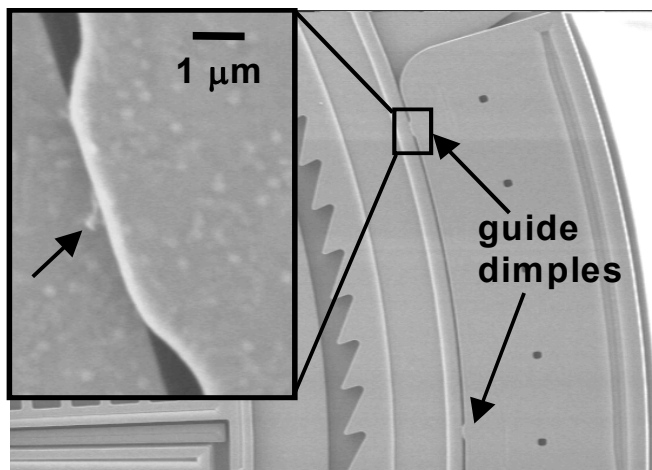


**Figure 10**. A FIB cross section of the dimple region of a TRA operated at $9.5 \times 10^5$ gear rotations.

signals were of the same voltage amplitude that is proportional to the force imparted to the ring gear, $F(V^2)$. The only difference is in the time that the force is applied. The higher frequencies impart a higher impulse to the ring gear, causing it to occasionally break adhesions, but more often engage the ratchet pawls.

*Wear Test*

In the wear test we were looking for failures where the ring gear was adhered to the alignment guides. We observed that in most cases, even though the ring gear didn't make a revolution at the inspection speed, it would run smoothly at high speed. The TRAs were run with the sine pulse shape with amplitude of 33 V. Data from this experiment are shown in Figure 11. The median number of rotations to failure was $9.8 \times 10^6$ with a slope parameter of 0.15. Also included in Figure 11 are data points using the failure criteria of no ratcheting at 5 Hz. These failures occur earlier than the adhesion failures at 333 Hz and would introduce a bimodal distribution (similar to the data in Figure 7) if included. This is further verifica-



**Figure 11**. The data from the wear test using an offset sine wave pulse of 33 V amplitude has a median number of rotations to failure of $9.8 \times 10^6$. Also plotted are failures at the 5-Hz criteria inspection test the actuator moves but the ring gear doesn't ratchet.



**Figure 9**. This SEM image shows the guide dimples in close contact with the ring gear. The magnified inset picture exhibits a speck of debris that may be from wear.
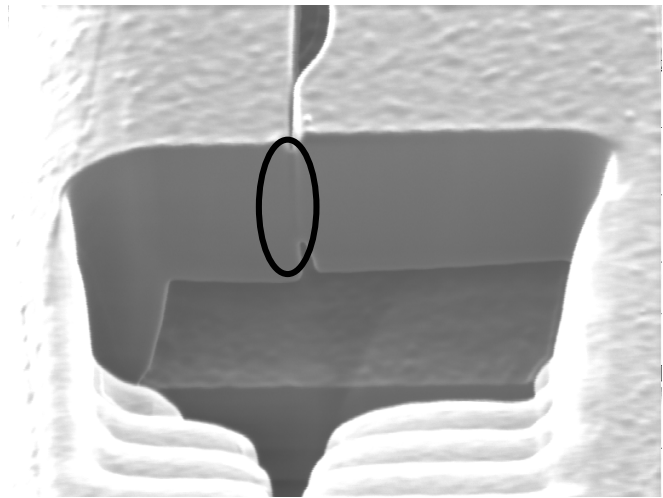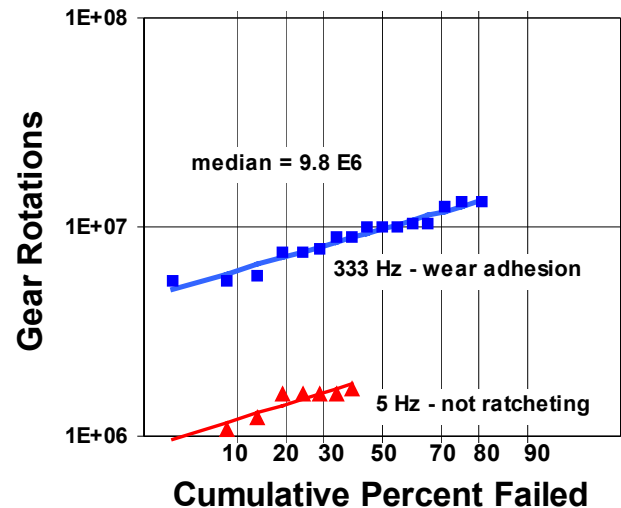
tion of the bimodal distributions in the frequency tests.

Several regions of the TRA are susceptible to wear. The surfaces most susceptible to wear include the ratchet pawls, the gear teeth, anti-reverse pawls, the ring gear, and alignment guide dimples. Wear debris was observed along the top surface of the dimple and to a small extent, along the top surface of the ring gear (Figure 12, a, b, and c). The debris along the surface of the ring gear was on the order of $1 \mu m^3$, while the amount of accumulated wear debris along the guides was measured as $5 \mu m^3$. The rubbing surfaces of the dimples and ring gear appear smooth.

The regions most susceptible to wear are the ratchet and anti-reverse pawls. No wear debris could be found along the ratchet teeth or ground plane. We observed wear debris on the ratchet top surfaces and tips of the pawls in many TRAs as illustrated in Figure 13. The worn material along the ratchet pawl is due to the rubbing of the pawl along the gear tooth while ratcheting along the ring gear.
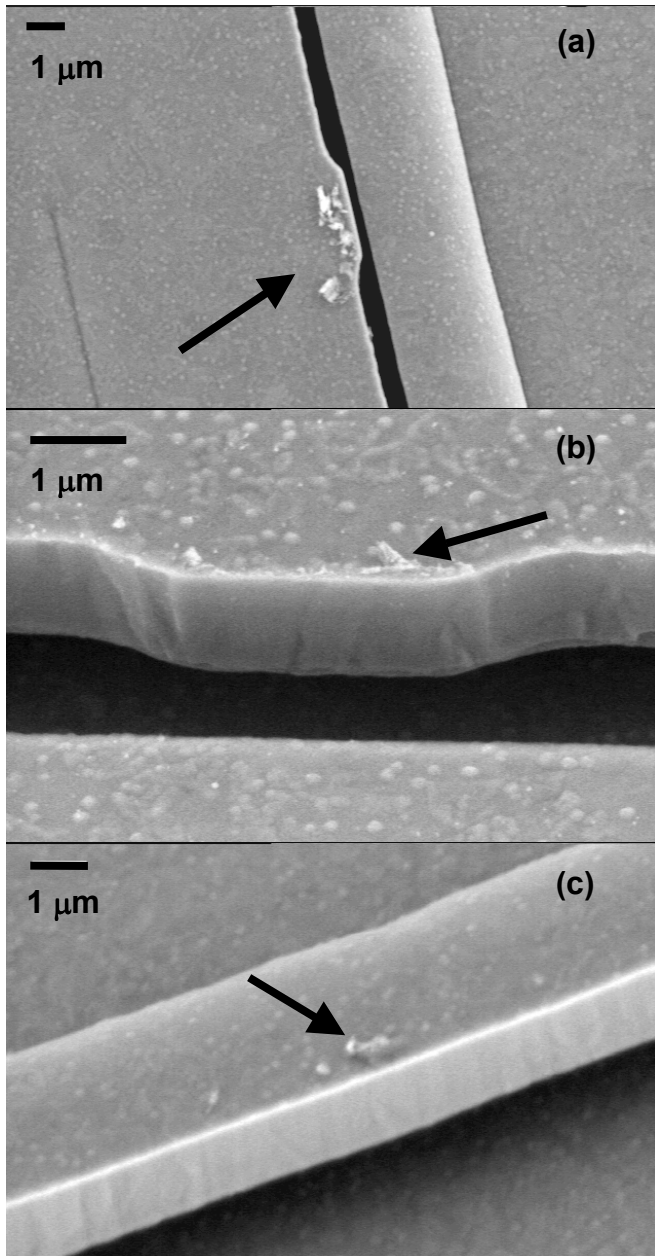
These rubbing surfaces produce wear debris while the ring gear is being driven. A measure of the debris accumulated on a ratchet pawl is $\sim 1 \mu m^3$. Assuming the amount of debris along each pawl is consistent, $3 \ \mu m^3$ of wear debris is located along the ratchet pawls. Note the absence of debris along the primary rubbing surfaces of the ratchet pawl. Several other pawls also did not reveal wear debris along these surfaces. The absence of wear may be due to the transfer of worn material to the gear teeth, or the accumulation of debris along the tips of the ratchet pawls. Although some wear debris is located along the ring gear, no wear debris was observed along the rubbing or exposed surfaces of the gear teeth. The majority of debris was found along the alignment guide dimples, ratchet pawls, and anti-reverse pawls.

Along with the ratchet pawls, the anti-reverse pawls also show signs of wear along the rubbing and impacting surfaces. As illustrated in Figure 14, wear debris is observed accumulating along the rubbing surfaces as well as the impacting surfaces. Wear along these
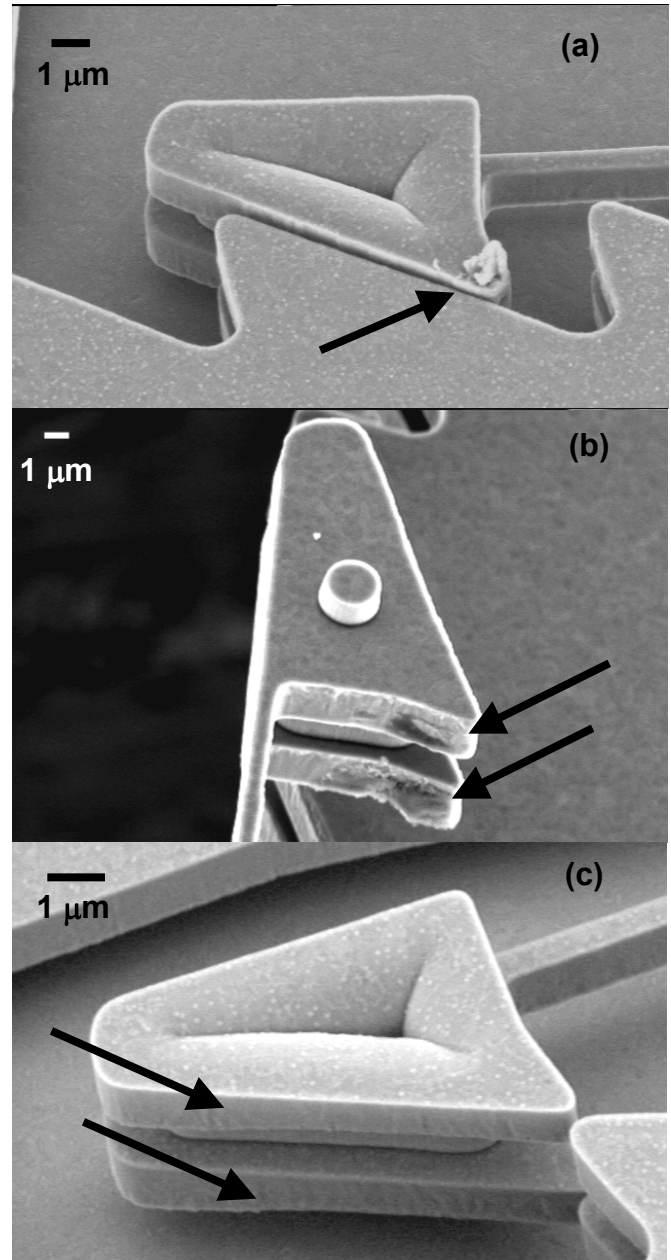


**Figure 12**. Wear debris present along (a) the top surface of an alignment guide dimple (arrow), (b) rubbing surface of the dimple, and (c) on the top surface of the ring gear. Note the smooth surfaces of the ring gear and the dimple.



**Figure 13**. Wear debris is found along (a) the top of a ratchet pawl (arrow) and (b) tip (arrows) in a bottom view of a ratchet pawl. No debris accumulated along (c) the rubbing surface (arrows).

surfaces is similar to the ratchet pawls where rubbing occurs along the inner ring gear teeth. Here, we see accumulation of wear debris along the rubbing surfaces, whereas debris was not observed along the rubbing surfaces of the ratchet pawls. A shorter polysilicon beam supports the anti-reverse pawls, which increases the normal force the pawl exerts along the gear teeth. Again, no wear debris is observed along the rubbing or exposed surfaces of the ring gear teeth. The amount of debris for a single anti-reverse pawl is $\sim 1$ $\mu m^3$. For a full TRA device, 3 $\mu m^3$ of debris is present along the three anti-reverse pawls, 3 $\mu m^3$ along the three ratchet pawls, 1 $\mu m^3$ along the ring gear, and 5 $\mu m^3$ along the alignment guide dimples, giving a total estimate of 12 $\mu m^3$.

Failure analysis of the bottom portion of the ring gear did not reveal any wear debris accumulating underneath the ring gear or along the ground plane. The accumulation of wear debris on the TRA can occur along many surfaces. The TRA has fewer enclosures than the microengine [4] to trap the material, which would wear the device even further.

*Wear Model for Failures*

The observation of wear debris and failures due to adhesion prompted us to develop a predictive model using the same approach as in earlier papers [4, 14]. Most models of wear between two contacting or rubbing surfaces include the relationship between the wear volume, *ΔV*, and the length of the motion producing the wear, *ΔL*, and *Fn*, the normal force between the contacting surfaces. The model can be expressed as [15]:

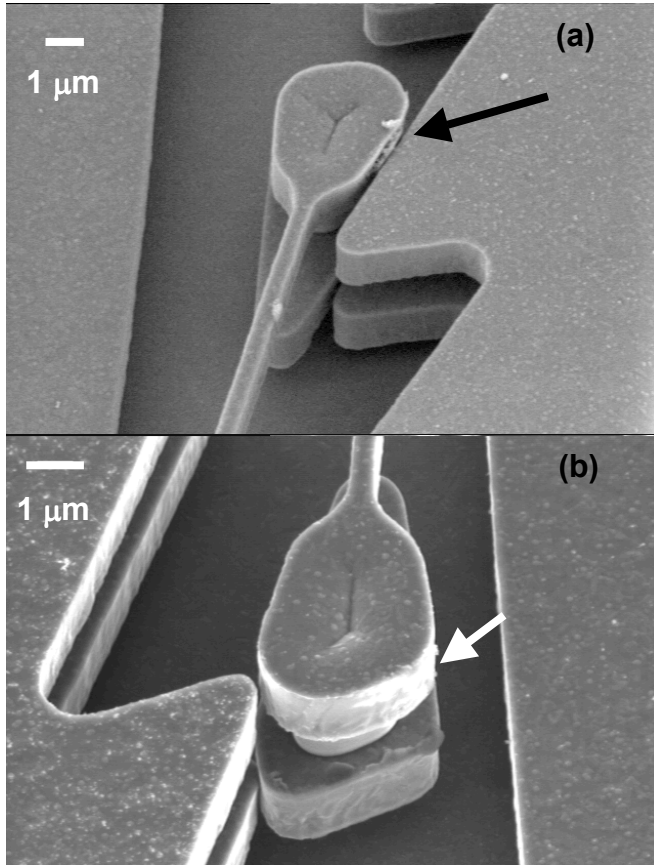**Figure 14.** Anti-reverse pawls revealed wear along (a) rubbing surfaces (black arrow) and (b) impacting surfaces (white arrow).

$$\Delta V = cF_n\Delta L \qquad (14)$$

where $c$ is a variable which is directly proportional to the wear coefficient and inversely proportional to the hardness of the material. The value of $c$ was determined using adhesive wear [14] and the equation, $c=K/9\sigma_{yp}$ where $K$ is the adhesive wear constant (value of $3.4 \times 10^{-7}$) and $\sigma_{yp}$ is the uniaxial yield strength ($1.2 \times 10^{-3}$ N/$\mu m^2$) measured for polysilicon in [16].

The volume of wear debris, *ΔV*, was estimated using the SEM. Table 2 shows the values used for obtaining the normal force from the wear equation. The sliding distance is the product of the circumference of rubbing surfaces and the number of revolutions to failure, $R_f$. The sliding distance was $2\pi rR_f$ for the guides (radius of 366 $\mu m$), but was $2(2\pi rR_f)$ the pawls because the teeth were composed of two layers (see Figure 13) with a radius of 340 $\mu m$. The median number of gear rotations to failure for the wear test was $10^7$. Using the total volume observed, we can then calculate the total normal force from the wear equation shown in the fifth column of Table 2. The source of the greatest error in the calculated $F_n$ is our value of $\Delta V$, which we estimate to be $\pm 1$ $\mu m^3$.

**Table 2**. Values used to calculate the normal force.

|  | Number | $\Delta V$ ($\mu m^3$) | $\Delta L$ ($\mu m$) | Total $F_{n\,wear}$ ($\mu N$) | $F_{n\,model}$ ($\mu N$) |
|---|---|---|---|---|---|
| Guides | 8 | 6 | $2.3 \times 10^{10}$ | $8.4 \pm 1.4$ | 2.7 |
| Ratchet pawls | 3 | 3 | $4.27 \times 10^{10}$ | $2.3 \pm 0.8$ | 1.1 |
| Anti-reverse pawls | 3 | 3 | $4.27 \times 10^{10}$ | $2.3 \pm 0.8$ | 2.1 |

We can also calculate the normal force using mechanics to compare to the wear model calculation. Agreement will validate the two methods. There are four guides located symmetrically around the perimeter of the ring gear. Each guide has two dimples separated by 14° of arc at a radius of 366 $\mu m$. Each dimple has a contacting length of 3.2 $\mu m$. We have determined that the ring gear can touch only one dimple at a time. We also observed wobble in the motion of the gear indicating that the gear bounced from dimple to dimple as it made rotations.

Examining the motion of the ring gear is the first step to derive the normal force associated with the guides. The ring gear has three pawl actuation points located 120° apart as shown in Figure 15. The pawls exert a tangential force on the ring gear for motion. The normal force of concern is that which is exerted on the guide dimples also located symmetrically around the ring gear. There is a 0.5-$\mu m$ gap between the ring gear and the guides which give rise to a wobble motion of the gear.

If all three tangential forces are equal, there will be no normal force due to cancellation of the force components. However, if one pawl engages earlier than the other, the potential for a large normal force exerted on the guides exists. Referring to Figure 15, we can calculate the normal component at the nearest guide for each of the three tangential forces. This would yield $F_t$, sin30 $F_t$, and sin60 $F_t$ for the actuation points at 12:00, 4:00, and 8:00 o'clock, respectively. The total normal force would then be $2.53F_t$. The total tangential force on the ring gear was measured and found to be 3.2 $\mu N$ [1], which determines $F_t$ to be 1.07 $\mu N$. Thus, the total normal force could be 2.7 $\mu N$.
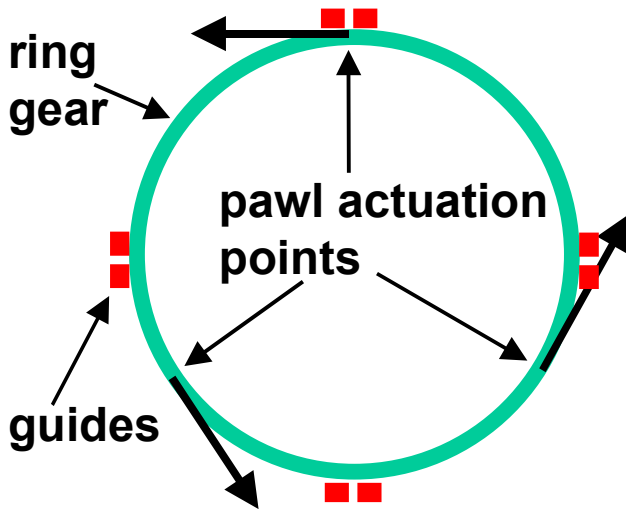
**Figure 15.** This diagram of the ring gear shows the pawl actuation points located symmetrically around the perimeter of the gear. The tangential force components and constraining guides are also shown.

The ratchet pawl is on the end of a 100-μm-cantilever beam that flexes (provides a normal force) for each actuation as illustrated in Figure 2. That force can be calculated using beam mechanics knowing that the maximum deflection ($\delta$) is 3.5 μm by the following equation,

$$F = \delta \frac{3EI}{L^3} \quad \text{where} \quad I = bt^3/12 \tag{15}$$

for a rectangular beam of width, $b$, and thickness, $t$. Using Young's modulus, $E$, of 165 GPa, $b$ of 2.5 μm, $t$ of 1.0 μm and $L$ of 100 μm, we arrive at a maximum force of 0.36 μN for normal operation. The total normal force from the ratchet pawls is 3 x .36 or 1.08 μN. In the same manner, the maximum normal force for the anti-reverse pawl can be calculated using a length of 77 μm and $b$ of 2.25 μm to yield 0.71 μN. Thus the total normal force for the anti-reverse pawls would be 2.1 μN.

Comparing the normal force from the wear equation to that from the model shows good agreement in the anti-reverse pawl values. This agrees with the fact that the anti-reverse pawl will always have one 'click' per tooth while the ratchet pawl does not. For the ratchet pawls, the normal force calculated from the wear equation is two times greater than that from the model. Additionally, for the guides, the normal force calculated from the wear equation is three times greater than that from the model. Although, the model underestimated the normal force from the guides, it's certainly within an order of magnitude. This was likely due to the static model. In reality, the ring gear is thrown into the guides and this has not been estimated. A complete dynamic model would be dependent on the initial boundary conditions and will not be attempted here. This static result is enough to convince us that we have good understanding of the wear mechanism.

### Comparison to Microengine

A major difference between wear in a TRA and the microengine is that the TRA debris can escape from the rubbing surfaces. In the microengine, all debris was trapped in the pin joint promoting three-body wear.

We have observed failures due to wear in the TRA with values of $10^7$ gear rotations at 333 Hz and roughly $10^6$ gear rotations at 1000

and 3000 Hz. In previous work [14], we have observed microengine failures at roughly $10^5$ for frequencies above 500 Hz and $10^9$ for frequencies below 500 Hz.

If we look at total linear displacement (Table 3), which is the circumference of the gear times the total number of gear rotations we find that the TRA is superior to the microengine at the higher frequencies and about the same as the microengine at lower frequencies.

**Table 3.** Total linear displacement (in meters) at failure

|  | Above 500 Hz | Below 500 Hz |
|---|---|---|
| TRA | 25,000 | 2500 |
| Microengine | 1300 | 2500 |

Design changes to the guide system to minimize the rubbing surfaces could certainly improve the TRA. A solution to the multiple ratcheting is also needed for reproducibility.

## CONCLUSIONS

We have observed wear as the dominant failure mechanism for this new actuator operated at high frequency. The wobble in the ring gear gives rise to a normal force at the alignment guide locations promoting this wear. When the TRA is operated at low frequency, the dominant failure mechanism appears to be the "wiggling" phenomena where a TRA cannot perform a complete revolution. This is due to misalignment of the ring gear that prevents engagement of the ratchet pawls. The major difference in the wear mechanism between the TRA and the microengine is that in the microengine, the debris is contained within the worn region that induces more wear within the microengine. In the TRA, once a surface is worn, the debris is not constrained to a specific location and may be removed by further frictional forces.

A model of the wear was developed similar to the microengine model. Comparing the normal force from the wear equation to that from the model shows good agreement in the anti-reverse pawl values and fair agreement in the ratchet pawl value. However, the model underestimated the normal force from the guides. This was likely due to the static model. In reality, the ring gear is thrown into the guides and this has not been estimated.

We have shown that the TRA is indeed a viable alternative to the microengine. More design work to eliminate the misalignment failures would improve the device.

## ACKNOWLEDGMENTS

## REFERENCES

[1] S. Barnes, S. Miller, S. Rodgers, and F. Bitsie, *"Torsional Ratcheting Actuating System,"* Inter. Conf. On Modeling and

Simulation of Microsystems, San Diego, CA, March 2000, pp.273-276.

[2] http://www.mems.sandia.gov/

[3] S. L. Miller, J. J. Sniegowski, G. LaVigne, and P. J. McWhorter, "Performance tradeoffs for a surface micromachined microengine", *Proceedings of SPIE Micromachined Devices and Components II*, **Vol. 2882**, Austin, October. 14-15, 1996, pp. 182-191.

[4] Danelle M. Tanner, William M. Miller, William P. Eaton, Lloyd W. Irwin, Ken A. Peterson, Michael T. Dugger, Donna C. Senft, Norman F. Smith, Paiboon Tangyunyong, and Samuel L. Miller, "*The Effect of Frequency on the Lifetime of a Surface Micromachined Microengine Driving a Load*," Proc. Of IEEE International Reliability Physics Symposium, 1998, pp. 26-35.

[5] J. A. Walraven, T. J. Headley, A. N. Campbell and D. M. Tanner, "*Failure Analysis of Worn Surface Micromachined Microengines*", SPIE Vol. 3880, 1999, pp. 30-39.

[6] R. Maboudian and R. T. Howe, "Critical Review: Adhesion in surface micromechanic structures," *Journal Vac. Sci. Technol.,* **B 15(1)**, Jan/Feb 1997, pp. 1-20.

[7] R. Maboudian and R. T. Howe, "Stiction reduction processes for surface micromachines," *Tribology Letters,* **3**, 1997, pp. 215-221.

[8] M. R. Houston, R. T. Howe, and R. Maboudian, *in 8$^{th}$ Int. Conf. On Solid-State Sensors and Actuators (Transducers '95) and Eurosensors IX,* **Vol.1** Stockholm, June 1995, pp. 210-213.

[9] R. L. Alley, R. T. Howe, and K. Komvopoulos, *Proceedings of the IEEE Solid-State Sensor and Actuator Workshop,* Hilton Head, SC, 1992, pp. 202-207.

[10] W. Geiger, B. Folkmer, U. Sobe, H. Sandmaier, W. Lang, *"New designs of micromachined vibrating rate gyroscopes with decoupled oscillation modes,"* Sensors and Actuators A, 66, 1998, pp.118-124.

[11] S. An, Y. S. Oh, K. Y. Park, S. S. Lee, C. M. Song, *"Dual-axis microgyroscope with closed-loop detection,"* Sensors and Actuators, 73, 1999, pp.1-6.

[12] D. M. Tanner, N. F. Smith, D. J. Bowman, W. P. Eaton, K. A. Peterson, " First Reliability Test of a Surface Micromachined Microengine Using SHiMMeR," *Proceedings SPIE Symposium on Micromachining and Microfabrication,* **Vol. 3224**, Austin, 1997, pp 14-23.

[13] Norman F. Smith, Danelle M. Tanner, Scot E. Swanson, and Samuel L. Miller, "*Non-destructive Resonant Frequency Measurement on MEMS Actuators*," Proc. Of 2001 IRPS, to be published.

[14] Danelle M. Tanner, William M. Miller, Ken A. Peterson, Michael T. Dugger, William P. Eaton, Lloyd W. Irwin, Donna C. Senft, Norman F. Smith, Paiboon Tangyunyong, and Samuel L. Miller, "*Frequency Dependence of the Lifetime of a Surface Micromachined Microengine Driving a Load*," Microelectronics Reliability Journal, **39** (1999) pp. 401-414.

[15] Ernest Rabinowicz, *Friction and Wear of Materials*, 2$^{nd}$ ed., New York, John Wiley & Sons, Inc., 1995.

[16] W. N. Sharpe, Jr, B. Yuan, R. Vaidyanathan and R. L. Edwards, "Measurements of Young's Modulus, Poisson's Ratio and Tensile Strength of Polysilicon," *Proc. MEMS 97, 10$^{th}$ IEEE Inter. Workshop on MicroElectroMechanical Systems*, pp. 424-429.